PHYSICAL REVIEW A **93**, 060302(R) (2016)

# Procedure for systematically tuning up cross-talk in the cross-resonance gate

Sarah Sheldon, Easwar Magesan, Jerry M. Chow, and Jay M. Gambetta
*IBM T.J. Watson Research Center, Yorktown Heights, New York 10598, USA*
(Received 23 March 2016; published 24 June 2016)

We present improvements in both theoretical understanding and experimental implementation of the cross resonance (CR) gate that have led to shorter two-qubit gate times and interleaved randomized benchmarking fidelities exceeding 99%. The CR gate is an all-microwave two-qubit gate that does not require tunability and is therefore well suited to quantum computing architectures based on two-dimensional superconducting qubits. The performance of the gate has previously been hindered by long gate times and fidelities averaging 94–96%. We have developed a calibration procedure that accurately measures the full CR Hamiltonian. The resulting measurements agree with theoretical analysis of the gate and also elucidate the error terms that have previously limited gate fidelity. The increase in fidelity that we have achieved was accomplished by introducing a second microwave drive tone on the target qubit to cancel unwanted components of the CR Hamiltonian.

DOI: 10.1103/PhysRevA.93.060302

The cross resonance (CR) gate is an entangling gate for superconducting qubits that uses only microwave control [1,2] and has been the standard for multiqubit experiments in superconducting architectures using fixed-frequency transmon qubits [3,4]. Superconducting qubits arranged with shared quantum buses [5] allow qubit networks to be designed with any desired connectivity. This flexibility of design also translates into a flexibility of control and many choices in entangling gate implementations. The CR gate is one choice of two-qubit gate that uses only microwave control, as opposed to using magnetic flux drives to tune two qubits into a specific resonance condition to entangle, as in the controlled-phase gate [6,7], or to tune a coupler directly [8–11]. The CR gate requires a small static coupling of the qubit pair that slightly hybridizes the combined system and one additional microwave drive. The relatively low overhead of the CR scheme (the additional control line is combined with a single-qubit drive at room temperature) makes it an attractive gate for use in quantum computing architectures based on planar superconducting qubits. Additionally, the CR gate is well suited to transmon qubits [12], which have become the superconducting qubit of choice due to promising long coherence and lifetimes [13,14], limited charge noise [15], and high single-qubit gate fidelities [16]. The microwave-only control allows the use of fixed-frequency transmons, further reducing the sources of possible noise [17]. Given all of these qualities, the CR gate has been a useful tool for application in multiqubit experiments, including demonstrations of parity measurements required for the surface code [3].

Despite the appeal of the CR gate, its implementation has been hindered by slow gate times. The CR gate relies on an always-on qubit-qubit coupling, but large couplings can lead to cross-talk between qubits. This leads to a trade-off between fast, high-fidelity two-qubit gates and high-fidelity simultaneous single-qubit gates. As a result, typical CR gates between transmon devices have resulted in gate times $> 300 \sim 400$ ns, with measured fidelities of 94–96% [4,18]. Here we describe improvements to the CR gate through a careful Hamiltonian analysis and novel tune-up procedure that reduce the gate time by a factor of 2 with corresponding fidelities over 99% (see Fig. 1). Our increased understanding of the CR Hamiltonian expands upon previous studies, which primarily used a simple qubit model [1,19]. We show that such models are incomplete and do not fully capture the dynamics of the complete two-transmon-qubit system.

The experimental system tested in this paper consists of two fixed-frequency transmon qubits coupled by a bus resonator as shown in Fig. 2. The qubit frequencies are 4.914 GHz (target qubit) and 5.114 GHz (control qubit) with anharmonicities of $-330$ MHz for both, and the bus frequency is 6.31 GHz. The coupling between the two qubits is estimated to be $J/2\pi = 3.8$ MHz for these parameters. The single-qubit gate fidelities measured with simultaneous randomized benchmarking [20] are $0.9991 \pm 0.0002$ for the target and $0.9992 \pm 0.0002$ for control. We characterize the two-qubit gate fidelities in the system by using interleaved randomized benchmarking (RB) [21,22]. For this measurement we first find the average fidelity per Clifford in the two-qubit system using standard randomized benchmarking [23], and then repeat the measurement interleaving the CR gate between random Cliffords in the sequence. The fidelities are extracted from exponential fits to the average over 35 random sequences each with a total length of 100 Clifford gates. By applying the theoretical Hamiltonian understanding of the next few sections, we were able to benchmark results showing a CR gate fidelity $f = 0.991 \pm 0.002$ for a 160-ns gate. This gate time includes 20 ns added by the single-qubit echo, which is buffered by two 10-ns delays. The CR pulses are rounded square pulses with Gaussian rise times of 15 ns.

The critical experimental technique for the improvement of the CR gate is an active cancellation pulse on the target qubit drive to eliminate unwanted interactions of the CR drive Hamiltonian, as shown in Fig. 1(a). Without this cancellation tone the CR gate fidelity for the same gate time is $f = 0.948 \pm 0.018$, demonstrating that the additional drive effectively cancels out the error terms of the CR Hamiltonian.

We measure the two-qubit gate fidelity as a function of gate time, plotted in Fig. 1(b) with the RB curves for the gate with the best measured fidelity. The fidelities reported here are calculated by fitting the probability of finding the target qubit in the ground state as a function of the RB sequence length. We have confirmed that the RB decay curves are consistent for both the control and target qubits, and we find that the decay rates are the same within error bars for either measurement. Indeed,

 

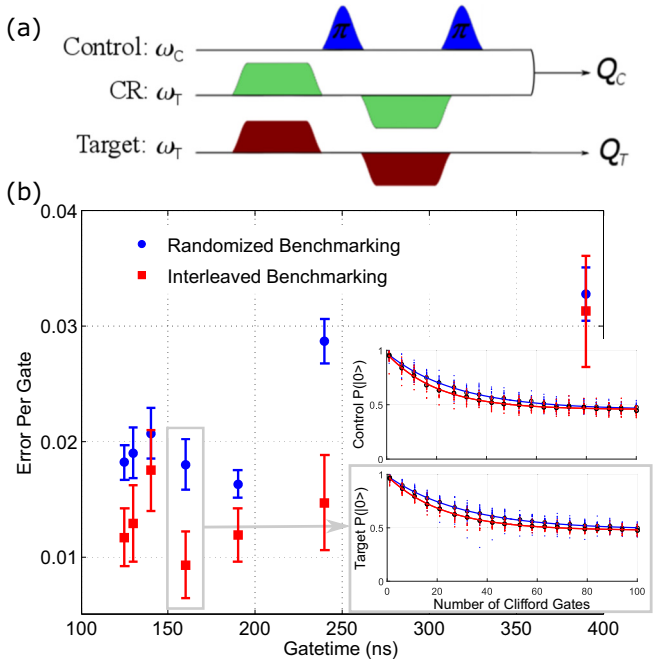


FIG. 1. (a) Schematic for the echoed cross-resonance gate with active cancellation on the target qubit. The $\pi$ pulse on the control is a 20-ns derivative removal via adiabatic gate (DRAG) pulse, and is buffered by two 10-ns delays. The CR pulses are flat-topped Gaussian pulses, with $3\sigma$ rise time where $\sigma = 5$ ns. (b) The error per gate found by randomized benchmarking (blue circles) and interleaved randomized benchmarking (red squares) as a function of gate time. The benchmarking decay curves for both the control and target qubit at the point with highest fidelity are highlighted in the inset. The error-per-gate data in the main figure correspond to measurements on the target qubit. We have performed checks on both qubits to confirm that the decay rates are the same on both qubits.

at the gate time with the lowest error rate we measure a fidelity of $0.991 \pm 0.002$ on the target qubit and $0.991 \pm 0.003$ on the control qubit. The gate time is the duration of the total echoed CR gate including the single-qubit echoing gates. While the fidelities improve as the gate time decreases from 400 to 160 ns, shorter gates appear to saturate. We suspect that leakage to

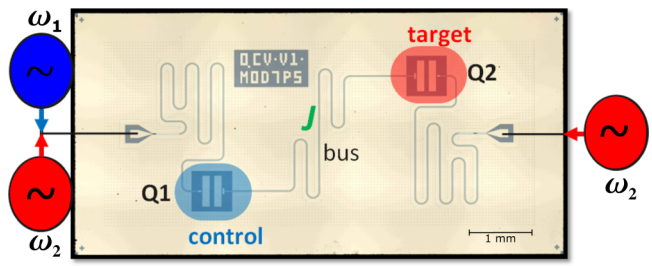


FIG. 2. The device consists of two transmon qubits coupled by a superconducting resonator. Each qubit has its own readout resonator. Single-qubit gates are applied directly to each qubit at its resonance frequency. The cross-resonance gate pulses are applied to the control qubit ($Q_1$) at the frequency of the target qubit ($Q_2$), while the active cancellation tone is applied on the same line as the target's single-qubit drive at $\omega_2$.

higher levels or drive-induced dephasing from the strong two-qubit drive may be the source of this saturation.

The addition of the cancellation drive on the target is the consequence of measurements and simulation of the CR Hamiltonian indicating single-qubit errors that are not fully refocused by the standard CR gate [e.g., the echoed sequence in Fig. 1(a) without the cancellation pulse on the target qubit]. We have developed an effective block-diagonal Hamiltonian model for the system dynamics under a CR drive that reveals the important contributions to the Hamiltonian on the qubit-qubit four-dimensional subspace. The method finds a unitary operator $T$ that block-diagonalizes the full system Hamiltonian $H$, $H_{\rm BD} := T^\dagger H T$, under the constraint that $T$ minimizes the distance to the identity operation $\|T - \mathcal{I}\|_2$ (hence $T$ affects the system as little as possible). The solution for $T$ is given by

$$T = X \frac{X_{\rm BD}}{\sqrt{X_{\rm BD} X_{\rm BD}^\dagger}}, \tag{1}$$

where $X$ is the eigenvector matrix of $H$ and is assumed to be nonsingular, and $X_{\rm BD}$ is the block-diagonal matrix of $X$.

In our implementation the different blocks correspond to the different states of the control qubit and off-resonant (higher energy) qubit subspaces. The model predicts $ZX$ and $IX$ components of similar magnitude, negligible $IZ$ and $ZZ$ contributions, and a large $ZI$ term arising from a Stark shift of the control qubit from off-resonant driving. The complete CR Hamiltonian has the structure

$$\mathcal{H} = \frac{Z \otimes A}{2} + \frac{I \otimes B}{2}, \tag{2}$$

where $A$ and $B$ are distinct unitary rotations on the target qubit.

Motivated by this understanding of the CR Hamiltonian, we have developed a protocol for experimentally measuring the CR Hamiltonian that allows us to determine the real error terms in the gate. This measurement is accomplished by turning on a CR drive for some time and measuring the Rabi oscillations on the target qubit. We project the target qubit state onto $x$, $y$, and $z$ following the Rabi drive and repeat for the control qubit in $|0\rangle$ and $|1\rangle$. Figure 3(a) contains an example of a complete set of such Hamiltonian tomography experiments. The last parameter plotted, $\|\vec{R}\|$, is the two-norm distance between Bloch vectors of the target qubit corresponding to the two states of the control qubit. This is defined as

$$\|\vec{R}\| = \sqrt{(\langle X\rangle_0 + \langle X\rangle_1)^2 + (\langle Y\rangle_0 + \langle Y\rangle_1)^2 + (\langle Z\rangle_0 + \langle Z\rangle_1)^2}. \tag{3}$$

When this quantity goes to zero, the two qubits are maximally entangled (unless the dynamics are completely mixed, but because $\|\vec{R}\|$ oscillates between zero and unity we believe this is not the case). We use $\|\vec{R}\|$ to estimate the gate length required to perform the entangling gate. We fit the set of Rabi oscillations that correspond to either state of the control qubit separately with a Bloch equation model function:

$$\dot{\vec{r}}(t) = e^{Gt}\vec{r}(0), \tag{4}$$

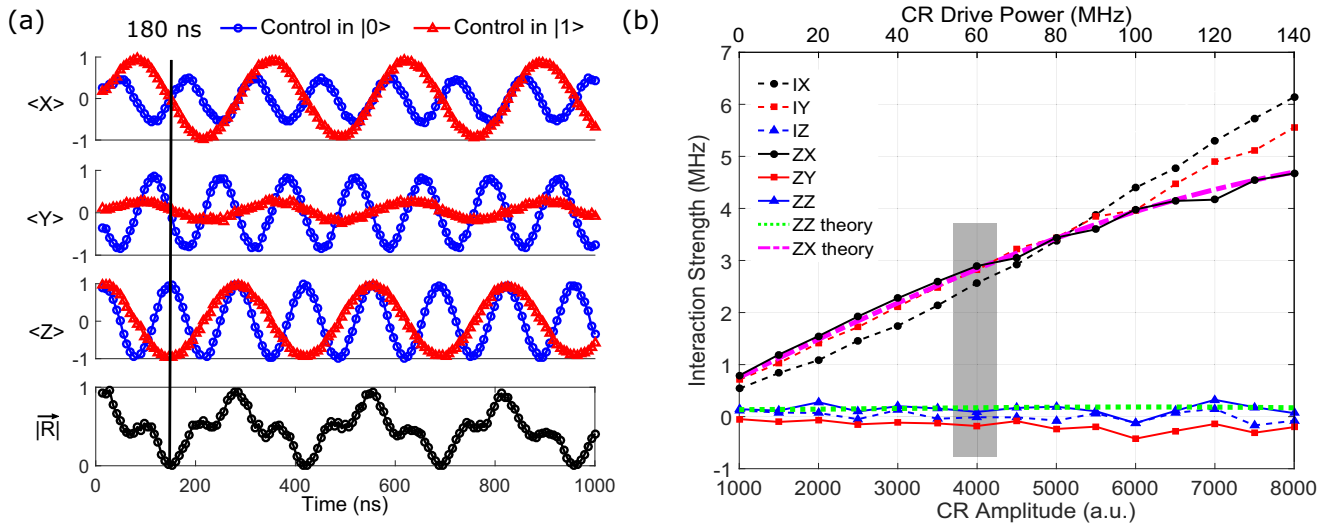


FIG. 3. (a) CR Rabi oscillations on the target qubit projected onto $x$, $y$, and $z$ for the control in $|0\rangle$ and the control in $|1\rangle$. The Bloch vector $R$ for the target indicates gate times of maximal entanglement at points when $R = 0$. (b) CR Hamiltonian as a function of the two-qubit drive amplitude including $IX$, $IY$, $IZ$, $ZX$, $ZY$, and $ZZ$. Theory predictions for $ZX$ and $ZZ$ are given as a function of the CR drive power on the upper $x$ axis. The grey shaded region corresponds to the data from (a) and later in Fig. 4.

with the matrix $G$ is defined as

$$\begin{pmatrix} 0 & \Delta & \Omega_y \\ -\Delta & 0 & -\Omega_x \\ -\Omega_y & \Omega_x & 0 \end{pmatrix}. \tag{5}$$

Here $\Delta$ is the control drive detuning, and $\Omega_{x,y}$ is the Rabi drive amplitude along $\{x, y\}$. $\vec{r}(t)$ is the vector composed of the measured expectation values as a function of the length of the applied Rabi drive, $[\langle X(t)\rangle, \langle Y(t)\rangle, \langle Z(t)\rangle]$. We find two generators, $G_{\{0,1\}}$, corresponding to the control qubit in either $|0\rangle$ or $|1\rangle$, characterized by the parameters $\Omega_x^{\{0,1\}}$, $\Omega_y^{\{0,1\}}$, and $\Delta^{\{0,1\}}$. From these parameters we derive the CR drive Hamiltonian in terms of the six possible interactions: $IX$, $IY$, $IZ$, $ZX$, $ZY$, $ZZ$. For example, $IX = (\Omega_x^0 + \Omega_x^1)/2$ and $ZX = (\Omega_x^0 - \Omega_x^1)/2$. By measuring the Bloch vectors as a function of time dependent on the state of the control, we can determine the operators $A$ and $B$ of Eq. (2). Note that this method of Hamiltonian tomography is applicable to any system with a Hamiltonian with the same form as Eq. (2). In addition, due to the symmetry of $\mathcal{H}$, this method scales efficiently for an $n$-qubit system since there are $n(n-1)/2$ different control-target qubit pairs and each pair requires six Rabi measurements described above.

We can vary the CR drive amplitude, perform the CR Rabi experiments, and extract the CR Hamiltonian using this Bloch equation fitting method. This provides a measurement of the CR Hamiltonian as a function of the two-qubit drive amplitude, as shown in Fig. 3. It is clear from this figure that components $IZ$ and $ZZ$ are small and independent of the drive power. These data were acquired with the CR drive phase set so that the $ZY$ contribution is small and the conditional component of the Hamiltonian consists only of $ZX$. The measured Hamiltonian parameters are consistent with the $ZX$ and $ZZ$ predicted by the effective Hamiltonian plotted in Fig. 3(b).

There is an unexpected feature in the experiment as there is also an $IY$ term present when the CR phase is set as above. We attribute this phase difference between conditional and single-qubit terms to classical cross-talk. Although such cross-talk has little effect on simultaneous RB since it is off-resonance, since the CR drive is applied at the frequency of the target qubit this cross-talk has a significant impact on the two-qubit gate calibration. The standard CR gate is performed using an echo to refocus $IX$, $ZZ$, and $ZI$, depicted in Fig. 1(a). The echoed scheme involves a $\pi$ pulse on the control qubit and a change of sign of the CR drive. If $IY$ terms are present, however, then the echo fails to completely refocus the unwanted interactions. In this case the $IY$ interaction does not commute with $ZX$ and all higher-order terms of the commutator will be on during the two-qubit gate.

The gate calibration procedure is based on these Hamiltonian measurements. Ultimately the goal is to tune up a $ZX_{90}$, which is a generator of a controlled-NOT (CNOT) with single-qubit Clifford rotations. The first step is to find the Hamiltonian parameters as a function of the phase of the CR drive [see Fig. 4(a)]. We use Fig. 4 to find the CR phase $\phi_0$ at which the $ZX$ component is maximized and $ZY$ is zero.

With the CR phase fixed at $\phi_0$ the two-qubit drive produces nonzero $IX$ and $IY$ components. We find the phase $\phi_1$ at which the single-qubit component $IY$ is zero. The correct phase for the cancellation pulse is $\phi = \phi_0 - \phi_1$, at which phase the single-qubit drive on the target matches $\tan^{-1}(IY/IX)$ for the two-qubit drive.

The second step is to set the cancellation pulse to the correct amplitude for canceling $\cos(\phi)IX + \sin(\phi)IY$. Again we measure the CR Hamiltonian, this time sweeping the cancellation pulse amplitude as shown in Fig. 4(b). If $IX$ and $IY$ are not zero at the same cancellation amplitude [$x$ in the schematic shown in 4(b)], then the cancellation phase is incorrect.

The CR-Rabi oscillations on the target qubit with the fully calibrated cancellation pulse (Fig. 5) are much closer to the oscillations expected for a $ZX$ drive. From Fig. 5 we see that the entangling gate is significantly faster than previous

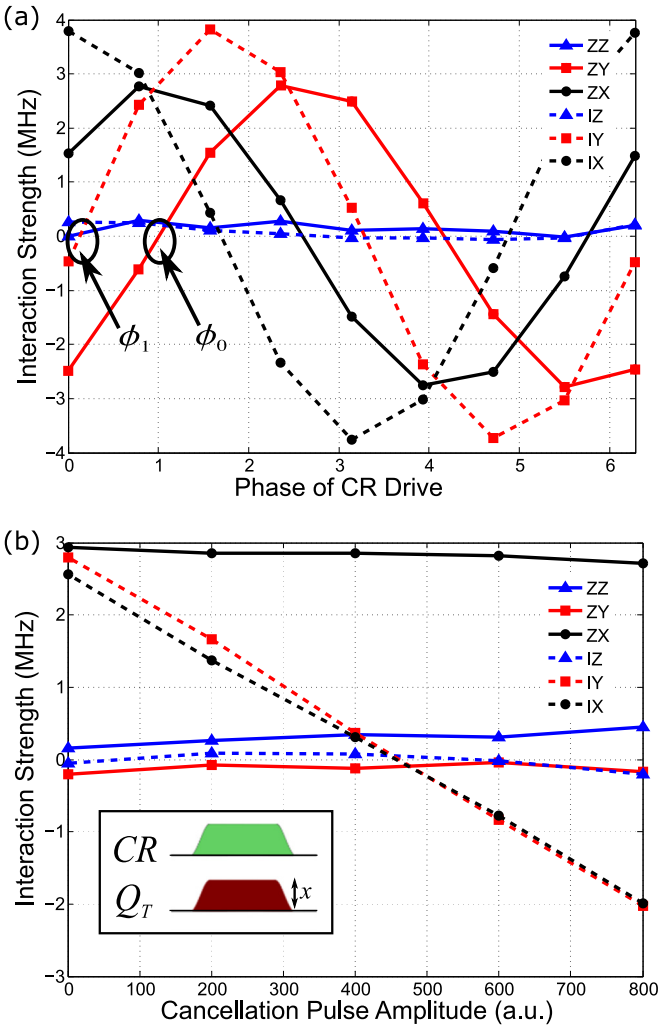


FIG. 4. (a) CR Hamiltonian parameters as a function of the drive phase: $ZZ$, $ZY$, $ZX$, $IZ$, $IY$, and $IX$. $\phi_0$ and $\phi_1$ are the phases at which $ZY$ and $IY$ are zero. The $ZX_{90}$ gate is calibrated by first setting the two-qubit drive phase to $\phi_0$ and the cancellation tone phase to $\phi_0 - \phi_1$. The second step is to find the correct amplitude of the cancellation tone. (b) The same Hamiltonian parameters plotted versus the active cancellation pulse amplitude ($x$, as shown in the pulse schematic in the inset). The correct amplitude for the cancellation pulse is the point at which $IX$ and $IY$ both cross zero. The CR amplitude for these data corresponds to that of the shaded region in Fig. 3(b).

cross-resonance gates; the $R$-vector goes to zero at 100 ns for the particular CR amplitude used. This is slightly slower than the entangling time of 83 ns that is predicted by the $ZX$ rate, which we attribute to the rise time of the pulse. The echoed gate time of 160 ns is consistent with the R-vector measurement as it includes the additional single qubit gate and the rise and fall of both halves of the CR echo. Additionally the oscillation of $\|\vec{R}\|$ are sinusoidal, unlike in Fig. 3. If the cancellation were perfect, there would be no oscillation of $\langle X\rangle$, and $\langle Y\rangle$ oscillations would have full contrast.

Plotting the same data on the Bloch sphere, as in Fig. 6, we can see the trajectory of the target qubit during the CR gate. The data in the top row of Fig. 6 are the target trajectories when the two-qubit echoed gate is applied with no active cancellation pulse. A perfect $ZX$ gate would result in a circle on the surface

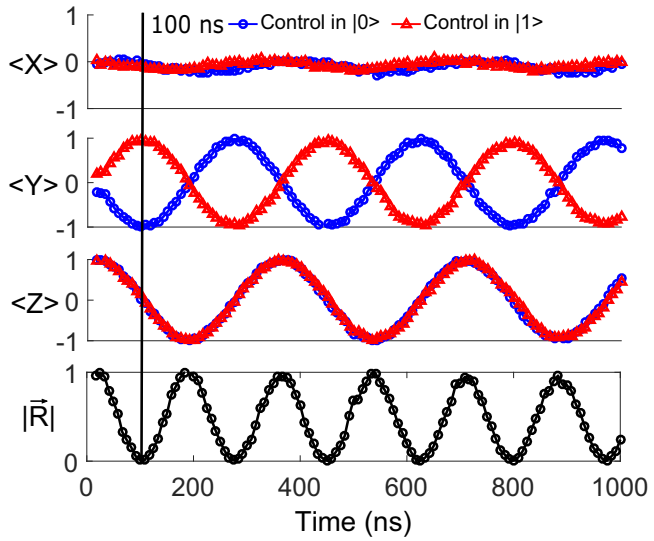


FIG. 5. CR Rabi experiments as a function of the CR pulse width after calibrating the active cancellation amplitude and phase. Shown are the expectation values $\langle X\rangle$, $\langle Y\rangle$, and $\langle Z\rangle$, and the Bloch vectors of the target qubit, $R$. Rabi experiments were performed with the control qubit in $|0\rangle$ and in $|1\rangle$.

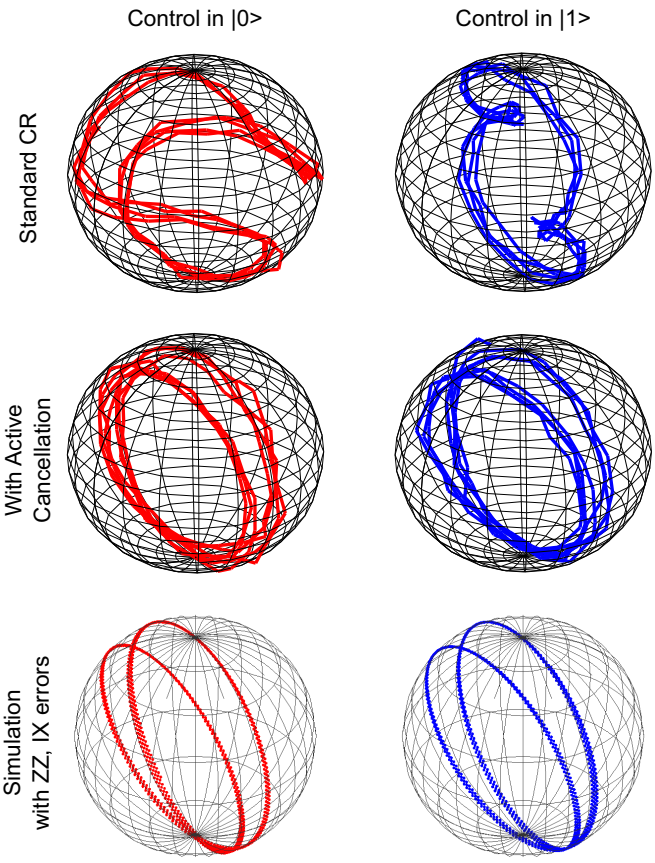


FIG. 6. Target qubit states plotted on the Bloch sphere during evolution during the echoed cross-resonance gate, when the control is in $|0\rangle$, and the control is in $|1\rangle$. Top row: echoed CR gate with no active cancellation. Middle: echoed CR gate with active cancellation on the target qubit. Bottom: simulations of the echoed cross resonance with small $IZ$ and $IX$ errors on the two-qubit drive.

of the Bloch sphere, but the echoed CR gate creates a more convoluted path on the Bloch sphere before an entangling gate is achieved. When the cancellation pulse is added (middle row), the picture is qualitatively closer to the ideal circle on the Bloch sphere, but still some error remains. Comparing that to a simulated echoed gate (bottom row), we find that the residual error is consistent with a $ZZ$ on the order of the $ZZ$ error we measure in the calibration sweeps and an order of magnitude smaller $IX$.

While the measured fidelity is higher than previously reported fidelities for CR two-qubit gates, it is still not yet limited by coherence. The limit placed on the fidelity by $T_1$ [$38 \pm 2$ $\mu$s ($41 \pm 2$ $\mu$s) for the control (target)] and $T_2$ [$50 \pm 4$ $\mu$s ($61 \pm 6$ $\mu$s)] for the two qubits is 0.996. There is evidence from studies of single-qubit gates that drive-activated dephasing may be a limiting factor for the error rates of gates at similar drive powers [16,24]. Even so, it appears from the CR Rabi data that coherent errors have not been fully eliminated in the CR gate.

While it is clear that some coherent errors remain on the cross-resonance gate, the inclusion of an active cancellation tone has produced a dramatic improvement in the two-qubit gate fidelity. The calibration procedure that we have developed has provided insight into the full CR Hamiltonian and revealed that a single-qubit phase shift due to cross-talk (either classical or quantum) is a significant source of error in the echoed CR gate. Future work will focus on shortening the gate times further by tuning up a CR gate without an echo and developing faster and more robust calibration procedures.

These improvements to the microwave-driven CR gate are encouraging for a quantum computing architecture built out of fixed-frequency qubits. With greater knowledge of the CR Hamiltonian, we are confident that further improvements can be made to reduce the two-qubit gate time and increase fidelity.

We acknowledge contributions from David McKay, Marcus Brink, Jim Rozen, and Jack Rohrs. This work was supported by ARO under Contract No. W911NF-14-1-0124.

[1] C. Rigetti and M. Devoret, Phys. Rev. B **81**, 134507 (2010).

[2] J. M. Chow, A. D. Córcoles, J. M. Gambetta, C. Rigetti, B. R. Johnson, J. A. Smolin, J. R. Rozen, G. A. Keefe, M. B. Rothwell, M. B. Ketchen, and M. Steffen, Phys. Rev. Lett. **107**, 080502 (2011).

[3] J. M. Chow, J. M. Gambetta, E. Magesan, D. W. Abraham, A. W. Cross, B. R. Johnson, N. A. Masluk, C. A. Ryan, J. A. Smolin, S. J. Srinivasan, and M. Steffen, Nat. Commun. **5**, 4015 (2014).

[4] A. Corcoles, E. Magesan, S. J. Srinivasan, A. W. Cross, M. Steffen, J. M. Gambetta, and J. M. Chow, Nat. Commun. **6** 6979 (2015).

[5] J. Majer, J. M. Chow, J. M. Gambetta, J. Koch, B. R. Johnson, J. A. Schreier, L. Frunzio, D. I. Schuster, A. A. Houck, A. Wallraff, A. Blais, M. H. Devoret, S. M. Girvin, and R. J. Schoelkopf, Nature **449**, 443 (2007).

[6] R. Barends, J. Kelly, A. Megrant, A. Veitia, D. Sank, E. Jeffrey, T. C. White, J. Mutus, A. G. Fowler, B. Campbell, Y. Chen, Z. Chen, B. Chiaro, A. Dunsworth, C. Neill, P. O'Malley, P. Roushan, A. Vainsencher, J. Wenner, A. N. Korotkov, A. N. Cleland, and J. M. Martinis, Nature **508**, 500 (2014).

[7] L. DiCarlo, J. M. Chow, J. M. Gambetta, L. S. Bishop, B. R. Johnson, D. I. Schuster, J. Majer, A. Blais, L. Frunzio, S. M. Girvin, and R. J. Schoelkopf, Nature **460**, 240 (2009).

[8] A. O. Niskanen, K. Harrabi, F. Yoshihara, Y. Nakamura, S. Lloyd, and J. S. Tsai, Science **316**, 723 (2007).

[9] R. C. Bialczak, M. Ansmann, M. Hofheinz, M. Lenander, E. Lucero, M. Neeley, A. D. O'Connell, D. Sank, H. Wang, M. Weides, J. Wenner, T. Yamamoto, A. N. Cleland, and J. M. Martinis, Phys. Rev. Lett. **106**, 060501 (2011).

[10] Y. Chen, C. Neill, P. Roushan, N. Leung, M. Fang, R. Barends, J. Kelly, B. Campbell, Z. Chen, B. Chiaro, A. Dunsworth, E. Jeffrey, A. Megrant, J. Y. Mutus, P. J. J. O'Malley, C. M. Quintana, D. Sank, A. Vainsencher, J. Wenner, T. C. White, M. R. Geller, A. N. Cleland, and J. M. Martinis, Phys. Rev. Lett. **113**, 220502 (2014).

[11] D. C. McKay, S. Filipp, A. Mezzacapo, E. Magesan, J. M. Chow, and J. M. Gambetta, arXiv:1604.03076.

[12] J. Koch, T. M. Yu, J. Gambetta, A. A. Houck, D. I. Schuster, J. Majer, A. Blais, M. H. Devoret, S. M. Girvin, and R. J. Schoelkopf, Phys. Rev. A **76**, 042319 (2007).

[13] A. A. Houck, J. A. Schreier, B. R. Johnson, J. M. Chow, J. Koch, J. M. Gambetta, D. I. Schuster, L. Frunzio, M. H. Devoret, S. M. Girvin, and R. J. Schoelkopf, Phys. Rev. Lett. **101**, 080502 (2008).

[14] R. Barends, J. Kelly, A. Megrant, D. Sank, E. Jeffrey, Y. Chen, Y. Yin, B. Chiaro, J. Mutus, C. Neill, P. O'Malley, P. Roushan, J. Wenner, T. C. White, A. N. Cleland, and J. M. Martinis, Phys. Rev. Lett. **111**, 080502 (2013).

[15] J. A. Schreier, A. A. Houck, J. Koch, D. I. Schuster, B. R. Johnson, J. M. Chow, J. M. Gambetta, J. Majer, L. Frunzio, M. H. Devoret, S. M. Girvin, and R. J. Schoelkopf, Phys. Rev. B **77**, 180502 (2008).

[16] S. Sheldon, L. S. Bishop, E. Magesan, S. Filipp, J. M. Chow, and J. M. Gambetta, Phys. Rev. A **93**, 012301 (2016).

[17] D. J. Van Harlingen, T. L. Robertson, B. L. T. Plourde, P. A. Reichardt, T. A. Crane, and J. Clarke, Phys. Rev. B **70**, 064517 (2004).

[18] A. D. Córcoles, J. M. Gambetta, J. M. Chow, J. A. Smolin, M. Ware, J. Strand, B. L. T. Plourde, and M. Steffen, Phys. Rev. A **87**, 030301 (2013).

[19] G. S. Paraoanu, Phys. Rev. B **74**, 140504 (2006).

[20] J. M. Gambetta, A. D. Córcoles, S. T. Merkel, B. R. Johnson, J. A. Smolin, J. M. Chow, C. A. Ryan, C. Rigetti, S. Poletto, T. A. Ohki, M. B. Ketchen, and M. Steffen, Phys. Rev. Lett. **109**, 240504 (2012).

[21] E. Magesan, J. M. Gambetta, B. R. Johnson, C. A. Ryan, J. M. Chow, S. T. Merkel, M. P. da Silva, G. A. Keefe, M. B. Rothwell, T. A. Ohki, M. B. Ketchen, and M. Steffen, Phys. Rev. Lett. **109**, 080505 (2012).

[22] J. P. Gaebler, A. M. Meier, T. R. Tan, R. Bowler, Y. Lin, D. Hanneke, J. D. Jost, J. P. Home, E. Knill, D. Leibfried, and D. J. Wineland, Phys. Rev. Lett. **108**, 260503 (2012).

[23] E. Magesan, J. M. Gambetta, and J. Emerson, Phys. Rev. A **85**, 042311 (2012).

[24] H. Ball, W. D. Oliver, and M. J. Biercuk, arXiv:1602.04551.